GEOPHYSICS, VOL. 71, NO. 6 (NOVEMBER-DECEMBER 2006); P. U77–U84, 6 FIGS., 5 TABLES.
10.1190/1.2345191

Seismic tomography studies of cover thickness and near-surface bedrock velocities

B. Bergman[1], A. Tryggvason[2], and C. Juhlin[2]

ABSTRACT

Reflection seismic imaging of the uppermost kilometer of crystalline bedrock is an important component in site surveys for locating potential storage sites for nuclear waste in Sweden. To obtain high-quality images, refraction statics are calculated using first-break traveltimes. These first-break picks may also be used to produce tomographic velocity images of the uppermost bedrock.

In an earlier study, we presented a method applicable to data sets where the vast majority of shots are located in the bedrock below the glacial deposits, or cover, typical for northern latitudes. A by-product of this method was an estimate of the cover thickness from the receiver static that was introduced to sharpen the image. We now present a modified version of this method that is applicable for sources located in or on the cover, the general situation for nuclear waste site surveys. This modified method also solves for 3D velocity structure and static corrections simultaneously in the inversion process. The static corrections can then be used to estimate the cover thickness.

First, we test our tomography method on synthetic data with the shot points in the bedrock below the cover. Next, we develop a strategy for the case when the sources are within the cover. The method is then applied to field data from five crooked-line, high-resolution reflection seismic profiles ranging in length from 2 to 5 km. The crooked-line profiles make the study 2.5 dimensional regarding bedrock velocities. The cover thickness along the profiles varies from 0 to 15 m. Estimated thickness of the cover agrees well with data from boreholes drilled near the profiles. Low-velocity zones in the uppermost bedrock generally correlate with locations where reflections from the stacked sections project to the surface. Thus, the method is functional, both for imaging the uppermost bedrock velocities as well as for estimating the cover thickness.

INTRODUCTION

One of the main objectives of reflection seismic surveying, in conjunction with the siting of potential nuclear waste repositories in crystalline rock, is the detection of subhorizontal to moderately dipping fracture zones at depth (Green and Mair, 1983; Kim et al., 1994; Juhlin and Palm, 1999). These zones are often difficult, if not impossible, to detect using only surface geophysics and geological mapping. Even when reflection seismic data have been acquired over potential sites, careful processing is necessary to image the fracture zones (Wu and Mereu, 1992; Juhlin, 1995). In northern latitudes, glacial deposits varying in thickness from a few meters to tens of meters are common. These deposits, or cover, with significantly lower velocities markedly delay the seismic waves as they approach the surface. Therefore, refraction static corrections that account for these delays are probably the most important initial step in processing reflection seismic data. Calculating of the refraction static corrections requires picking of first-break traveltimes, generally a tedious process. After application of the refraction statics, the first-break traveltimes normally are not used again.

In a previous paper (Bergman et al., 2004b), we showed how the first-break traveltimes could be used to produce a tomographic image of the shallow (0–400 m) velocity field below a reflection seismic profile designed to image depths down to 10 km. An important result from this work was that a sharper image of the velocity field was obtained if a receiver static correction was included in the inversion process. A source static correction was not necessary because

Manuscript received by the Editor November 11, 2004; revised manuscript received April 18, 2006; published online October 3, 2006.
[1]Formerly Uppsala University, Department of Earth Sciences, Uppsala, Sweden; presently Geological Survey of Sweden, Department of Marine geology and geophysics, Villavägen 18, 752 37 Uppsala, Sweden. E-mail: bjorn.bergman@sgu.se.
[2]Uppsala University, Department of Earth Science, Villavägen 16, 752 36 Uppsala, Sweden. E-mail: ari.tryggvason@geo.uu.se; Christopher.juhlin@geo.uu.se.

all shots were in, or close to, bedrock. A by-product of the study was the receiver delay times. These delay times correlated well with the cover thickness as found by shot-hole drilling. This observation suggested that the same inversion strategy could be used to map the depth to bedrock along with the velocity field in studies where the sources are at or close to the surface. Traditionally, such mapping would be carried out using refraction seismic survey geometries with a denser receiver spacing, but a much sparser source spacing than in reflection seismic surveys. The denser source spacing of reflection seismic surveys implies that seismic tomography is more likely to be successful, as it is in crosswell surveys (Yamamoto, 2001). However, tomography has been applied successfully even with sparse-source spacing on the global scale, e.g., using peaceful nuclear explosions (Nielsen et al., 1999). Tomography has also been used in time-lapse studies (Vesnaver et al., 2003) and in wave-equation datuming (Flecha et al., 2004).

Our first-break tomographic inversion routine solves simultaneously for bedrock velocities and source or receiver corrections, and we refer to it as tomography inversion with statics, or TIS. Because statics are solved for in the velocity inversion, the resulting velocity models have less smearing of low velocities from the cover into the bedrock below. In tomostatics, a related method, statics are calculated as the traveltime through a vertical column from a velocity model determined using a tomographic inversion from a source or receiver position to a datum (Zhu et al., 1992; Squires et al., 1994). The difference between tomostatics and our method is that in the former, the statics are calculated after the inversion for the velocity field, whereas in our method, the static corrections are solved for simultaneously with the velocity field. For this reason, in high-resolution imaging and shallow studies, our method should be expected to yield a better solution because the velocity model will not be degraded as much by smearing.

We show how to incorporate source statics into TIS. We then test our method and the tomostatics method on synthetic traveltime data. Finally, we apply our method to real reflection seismic data acquired at one of the potential sites for storage of high-level radioactive waste in Sweden (SKB, 2002). Depth to bedrock and bedrock velocity are mapped along five different profiles. The main purpose of this study is to improve the estimate of depth to bedrock and the estimates of the uppermost bedrock velocity, not to improve the stacked reflection seismic section. Based on the results from TIS, and boreholes drilled near the profiles, we suggest that the correlation length of the bedrock topography is a few tens of meters.

METHOD

When seismic waves pass through the low-velocity glacial deposits covering the bedrock, large delays may arise. This low-velocity cover may be several tens of meters thick and may have a velocity one-tenth or less of that of the underlying bedrock. In principle, this low-velocity cover can be modeled using a fine grid spacing. However, at the cover-bedrock interface, there will be a smearing of the velocities in the model because of the smoothing constraints applied in tomographic inversion. Smoothing constraints of some form are often applied in this kind of nonlinear, mixed determined problem. This smearing of the velocity field at the cover-bedrock interface can produce artifacts in the final model, hindering a reliable interpretation. Although other types of constraints exist, smoothing constraints are used in this study. Throughout this study, we have used the same smoothing constraints in all inversions. To avoid smearing artifacts in the velocity model while retaining the robustness obtained by the smoothing constraints, we simultaneously invert for static time shifts along with velocities. The static corrections are surface consistent and absorb the short-wavelength variations in traveltimes. Here we have assumed that most of the short-wavelength variation arises when passing through the low-velocity cover. The size of this static correction depends on not only the cover thickness but also the velocity model. The initial velocity model is assigned by a trial-and-error fitting of the first-break traveltimes with statics to a 1D velocity function. This 1D velocity function is then used as the starting model in further iterations. With this approach, we have replaced the low-velocity layer covering the bedrock with a correction term in the traveltimes of the recorded data. The velocity in the top of the model will be that of the bedrock. This will compromise the raypaths at shorter offsets; but where the source-receiver distance is large compared to the layer thickness, this will have little effect. The formalism needed to solve jointly for a static time term and seismic velocities starts with the nonlinear line integral for controlled source seismic tomography describing the traveltime t_{mod} for one source-receiver pair. This equation can be written as

$$t_{\mathrm{mod}} = \int_{l[u(\mathbf{p})]} u(\mathbf{p})\,dl, \tag{1}$$

where $u(\mathbf{p})$ is the slowness (inverse of velocity) as a function of the spatial position $\mathbf{p}$ and l is the raypath, which is itself a function of $u(\mathbf{p})$ (Benz et al., 1996). By linearizing and parameterizing equation 1 about a starting model with uniformly sized model blocks, we get (see equation 2 in Benz et al., 1996)

$$t_{\mathrm{obs}} - t_{\mathrm{mod}} = r_{ij} = s_{ij} + \sum_{n}^{N} \frac{\partial\, T_{ij}}{\partial\, u_n}\Delta u_n,\ i = 1,\ \ldots,\ I,$$
$$j = 1,\ \ldots,\ J, \tag{2}$$

where r_{ij} is the residual based on the starting model for all I sources and J receivers, s_{ij} is the static correction to the traveltime $\partial T_{ij}/\partial u_n$ are the partial derivatives of traveltime T_{ij} with respect to the slowness in block n along the raypath, and Δu_n is the change in slowness in model block n that is to be found for all N blocks.

From equation 2, we see that we have one unknown static-correction term for every data point. If the sources are placed in or near the bedrock interface and the receivers at the surface, as in the case of our previous study (Bergman et al., 2004b), then it is a valid approximation to ignore the contribution from the source location and assume that the static correction is dependent on the receiver location only (s_j):

$$s_{ij} \approx s_j. \tag{3}$$

The equations for all rays from source i can be written as a system of equations,

$$\mathbf{s} + \mathbf{D}_i\Delta\mathbf{u} = \mathbf{r}_i, \tag{4}$$

where $\mathbf{r}_i$ is the vector of traveltime residuals, $\Delta\mathbf{u}$ is the slowness perturbation, and $\mathbf{D}_i$ is the matrix of all distances d_n for all raypaths recorded from this source. The procedure to solve this coupled system is described by Pavlis and Booker (1980) with examples for local earthquake tomography. Equation 4 is solved by first using singular-value decomposition (SVD) to separate the static correction from the slowness model and to solve for them simultaneously. The size of the

I number of SVD systems is determined by the number of receivers J. The application of SVD to equation 4 will cause the static correction term to vanish and equation 4 is reduced to

$$\mathbf{D}_i'\Delta\mathbf{u} = \mathbf{r}_i'. \tag{5}$$

Solution stability and some degree of artifact suppression is achieved by adopting the constraint of demanding the Laplacian of the slowness perturbation field to be zero. The final system of equations to be solved can now be written as

$$\begin{bmatrix} \mathbf{D}' \\ k\mathbf{L} \end{bmatrix} \Delta\mathbf{u} = \begin{bmatrix} \mathbf{r}' \\ 0 \end{bmatrix}, \tag{6}$$

where k is a constant scaling the importance of the smoothing constraint and $\mathbf{L}$ is the Laplacian smoothing operator (see equation 3 in Tryggason et al., 2002). Our tomography inversion routine iteratively updates a velocity model based upon the residual time difference between the first-break traveltimes and the computed traveltimes in the model. In each iteration, the isochrones are computed using a first-order, finite-difference approximation of the eikonal equation (Hole and Zelt, 1995); then raypaths for the present velocity model are calculated by ray tracing backward from receiver locations perpendicular to isochrones (Hole, 1992). The inversion problem is then solved using the Paige and Saunders (1982) conjugate gradient solver LSQR. Convergence generally is achieved after a few iterations, and in this study, all inversions were run for six iterations. The initial model is critical for the convergence rate and the precision of the final model as the problem is nonlinear (Kissling, 1988; Kissling et al., 1994).

It is obvious that, if both sources and receivers are situated in the same cover layer above the bedrock, as in the area presented in this paper, the task becomes numerically impractical to solve. After the decoupling of the static corrections from the slowness model, a second application of SVD would have to be made to separate the statics from the sources and from the receivers. The size of the SVD system would then be the same size as the number of data, i.e., the number of rays. With a typical seismic survey with tens-or hundreds-of-thousands of traces, the vast memory requirements of storing the SVD matrices, the errors of the eigenvalues, and the eigenvectors in the SVD would be prohibitive. However, if the sources are located next to the receivers, the static corrections are, in principle, the same. This suggests the possibility of an alternative iterative scheme for cases when the sources are placed in or on the low-velocity layer.

The scheme for every iteration is as follows: First, one initial TIS inversion is run to calculate receiver static corrections, but without updating the velocity field. Second, the obtained static corrections are divided equally between the receiver and the sources, assuming surface consistency and a medium velocity as in the top layer. Finally, a tomographic inversion without simultaneous static calculations is run to update the velocity model.

SYNTHETIC DATA

A synthetic data set was generated to investigate the performance of our method to solve for the thickness of the low-velocity cover and the underlying crystalline bedrock velocities. When generating synthetic data, we only calculate traveltimes for the first arrivals; synthetic seismograms are not generated. First, we generated a velocity model that has characteristics similar to the field site. The synthetic profile followed a crooked line (Figure 1) and had a nominal source and receiver spacing of 10 m. The source-receiver geometry was the same as the field data in the study with an end-on spread type on the left side becoming a shoot-through on the right side as the spread was moved. The velocity model used was two dimensional with no variations in the x-direction (Figure 1), resulting in a 2.5D problem because the acquisition geometry is along a crooked line.

The low-velocity cover contained two layers: an upper low-velocity layer (500 m/s) and a deeper layer with higher velocities ranging from 500 m/s at the top of the layer to 3000 m/s at the base at those locations where it is thickest. The velocity at the top of the bedrock was fixed to 4500 m/s (Figure 1). The bedrock topography followed the surface topography but varied slightly more in amplitude. Two sets of synthetic traveltimes were generated. Set I had shot points 2.9 or 3.5 m beneath the cover-bedrock interface. Set II had all shot points in the cover at 0.9 or 1.5 m below the surface.

The set I shot points at 3.5 m depth below the interface were located at the same positions as those that were at 1.5 m depth in set II. Set I was used as a reference because it corresponds to the conditions and geometry in the study of Bergman et al. (2004b). Set II was considered the more general case because it is often not possible to place all shots in the bedrock. It should be emphasized that for set I, the primary purpose of the inversion is to derive as good a velocity model as possible for the top of the bedrock because we essentially know the cover thickness from the shot point locations. For set II, the thickness of the low-velocity cover is unknown; therefore, both the cover thickness and the bedrock velocity are targets for the inversion. The synthetic traveltimes were generated by ray tracing through a very fine grid with cell sides of 2 m and with a total size of $250 \times 2100 \times 520$ m, resulting in 34.125 million model blocks. For the inversion, a much coarser grid was used, with the inversion model parameters optimized for the station spacing (nominally 10 m along the y-axis; Table 1). The model block size used in the inversion results in about the same number of covered blocks as the number of

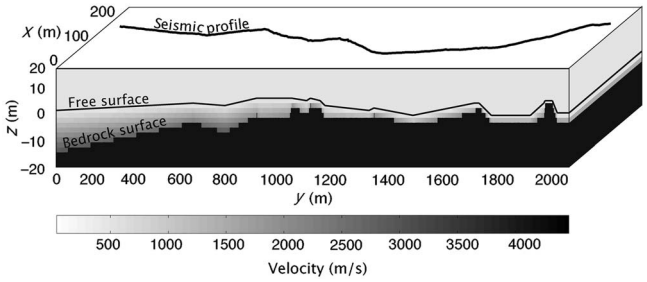

Figure 1. Synthetic velocity model representing unconsolidated sediments covering the crystalline bedrock. The line on the vertical surfaces shows the surface topography. The crooked acquisition line is shown on the horizontal surface.

Table 1. Parameters used for inversion of the synthetic data.

Parameter for the inversions	$x \times y \times z$
Ray-tracing grid cell size	$5 \times 5 \times 5$
Grid cell size of inversion	$50 \times 10 \times 5$
Total size of model	$250 \times 2100 \times 520$
Number of cells in model	109,200

rays. A decrease in the inversion block size only increased computation times without improving the data fit.

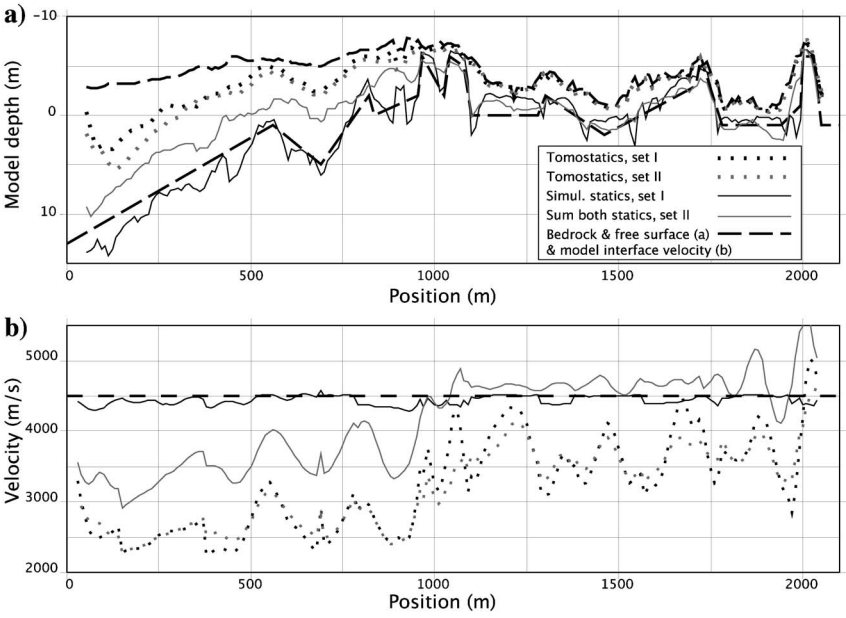

Figure 2. (a) Estimated low-velocity layer cover thickness from tomostatics only (dotted lines), tomography inversion with statics (TIS) (black line), and sum of TIS and tomostatics (gray line). (b) Velocities at the cover-bedrock interface. Solid lines show velocities from TIS and dotted lines from tomostatics. Black lines identify results from inversion of data set I and gray lines from data set II. Surface, bedrock surface in (a) and true cover-bedrock interface velocity in (b) are shown as dashed lines.

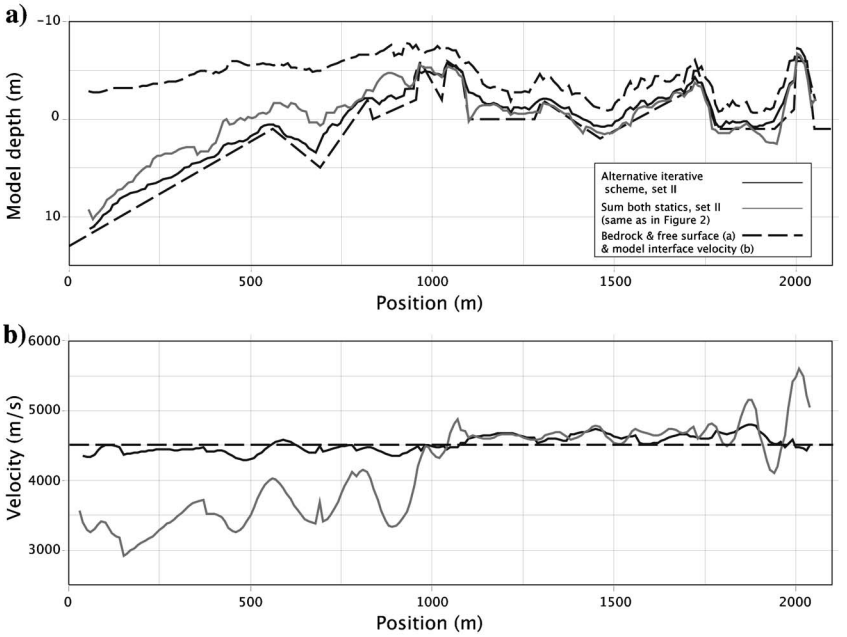

Figure 3. (a) Estimated low-velocity layer cover thickness from TIS with all statics applied to the receivers (gray), statics applied to receivers and sources (black) in a surface-consistent manner. (b) Velocities at the cover-bedrock interface. All statics applied to the receivers (gray), statics applied to receivers and sources (black) in a surface-consistent manner.

Inversion of the synthetic data

The inversion of synthetic data set I proved that very robust and good estimates of the cover thickness were obtained. With all shots positioned in the bedrock, the only delay times from the cover were at the receivers at the end of the raypaths. The velocities at the cover-bedrock interface in the inverted model were only slightly different from the velocity in the initial synthetic model. The inverted model had a mean velocity at the boundary of 4420 m/s with a maximum deviation of ±150 m/s compared to the true velocity of 4500 m/s (Figure 2b). The estimated unconsolidated sediment thickness calculated from the TIS receiver corrections matches the cover thickness of the model well (Figure 2a).

In the tomography inversion for data set I without simultaneous static corrections, the velocity inversion attempts to model the cover itself. However, the velocity in the cover is higher than in the initial model, and the bedrock velocity at the top of the bedrock interface is too low (Figure 2b). The smoothing constraints cause the deviation from the true model velocities in the cover to be much larger than for the velocities in the bedrock because of the limited thickness of the cover. This results in velocities that are too high near the surface, causing the tomostatics to become too small (Figure 2a). The datum used in estimating the tomostatics (Zhu et al., 1992; Squires et al., 1994) was set to twice the maximum bedrock depth in the initial model. Setting the datum to a deeper level did not improve the statics. The tomostatic results are particularly poor on the left side containing an end-on spread.

Inversion of synthetic data set II, with the shots within the cover, proved more difficult. In this case, the time delays caused by the cover are associated with both the source and the receiver positions. By combining the TIS receiver corrections and the tomostatics calculated from the velocity model, we can obtain an estimated cover thickness that correlates well with the true thickness of the low-velocity layer (gray solid line in Figure 2a). However, because of the remaining traveltime delays, the velocities are smoothed across the cover-bedrock interface. As in the case of data set I, the estimated depth to bedrock is too low when computed from tomostatics alone (gray dotted curve in Figure 2a). Furthermore, for this configuration, the velocities near the cover-bedrock interface are even more smeared than when all shots were placed in bedrock (data set I).

In the inversion results of data set II, the thickness of the cover is generally much greater than the depth of the shot points. This suggests the use of the alternative iterative scheme described earlier for set II. Applying the alternative strategy gives nearly the correct inverted velocities at the sediment/bedrock interface (black line in Figure 3b).

Although the alternative iterative scheme produces the best results, there exists some high-frequency noise for the cover thickness (Figure 3a). This noise is probably from the difference in model cell size between the model used for generating synthetic traveltimes and the cell size used in the inversion.

In summary, when shot points are below the cover-bedrock interface (data set I), TIS works well. The correct velocities at the cover-bedrock interface are obtained along with a good estimate of the cover thickness. For shots in the cover (data set II), best results are obtained by the alternative iterative scheme.

FIELD DATA

In spring 2002, five high-resolution reflection seismic profiles (Figure 4) were acquired in the Forsmark area, Sweden (Juhlin and Stephens, 2006). The Forsmark area, located in Precambrian bedrock, is a potential site for storage of high-level nuclear radioactive waste (SKB, 2002) at a depth of about 500 m (Ericsson, 1999). Seismic activity is very low in the area, and no active faulting has been observed. Two major shear zones surround rather homogeneous granitic bedrock at the site. Less prominent fracture zones are also present (Juhlin et al., 2002; SKB, 2002). Most of the bedrock is covered by glacial till with a thickness up to approximately 15 m (Lundin et al., 2004). The reflection seismic data were recorded with the acquisition parameters in Table 2. The small charge size produced high-frequency signals of about 150 Hz, allowing accurate automatic picking followed by manual inspection and corrections of the first breaks to the order of 1–2 ms. In the case of uncertainty of a first-break time, the trace was excluded from the study. From the more than 132,000 traces recoded, first breaks were picked on 87% of these, or about 115,000 traces. These first breaks were used in the tomography (Table 3).

None of the profiles had enough shots in bedrock for a one-step inversion using solely TIS. Therefore, seismic tomography was performed on each of the five profiles using the alternative iterative scheme outlined earlier. To obtain control of the velocity of the cover

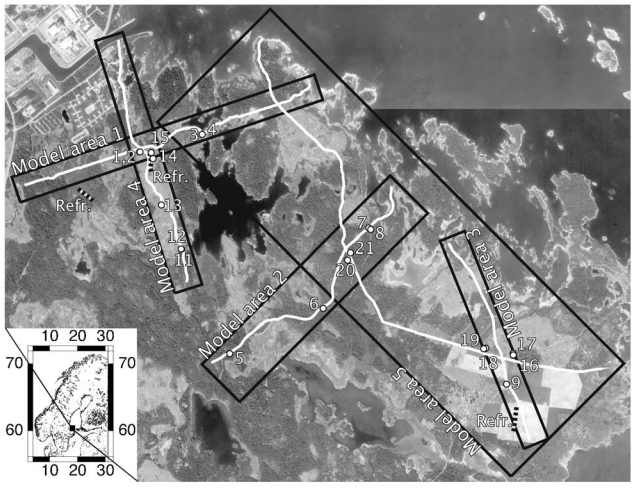

Figure 4. Reflection seismic profiles (white lines) and model areas (black frames). Refraction seismic profiles are shown with black and white dashed lines. Boreholes with recorded depth to bedrock are marked with white circles. On the aerial photo, the darkest areas are the sea or lakes, intermediate grays are forests, and lighter gray corresponds to wetland or agricultural areas.

(Bergman et al., 2004a), three short (a few hundred meters) conventional refraction seismic profiles were shot (Figure 4). The refraction seismic data had a typical frequency of about 125 Hz and a record length of 250 ms using a sampling rate of 0.25 ms. The refraction surveys were shot with 24 channels using a 1-m geophone separation. On all three sites, at least three layouts were placed. For each layout, one near shot and three far shots were made on each side of the individual layout. From these measurements, a 1D velocity function for the cover was defined (Table 4).

Error estimates of the inversion regarding cover thickness

The data were picked with an accuracy of 1–2 ms. For bedrock velocities starting at about 4000 m/s, the smallest structure that could possibly be resolved was on the order of 4 m. We chose to compute traveltimes for the inversions on a 5-m uniform grid, commensurate with the accuracy needed. The synthetic traveltime data were computed on a 1-m uniform grid to allow for the details in the cover-bedrock interface to be represented properly. The static cor-

Table 2. Acquisition parameters.

Parameter	Value
Spread type	End-on/shoot-through
Number of channels	100
Near offset	20 m
Geophone spacing	10 m
Geophone type	28-Hz single
Shot:	
Spacing	10 m
Size, bedrock/till	15 g/75 g
Hole diameter, bedrock/till (casing)	12 mm/16.9 (plastic) –18 mm (metal)
Nominal charge depth, bedrock/till	0.90 m/1.50 m
Nominal fold	50
Recording instrument	SERCEL 348
Sample rate	1 ms
Field low cut	8 Hz
Field high cut	250 Hz
Record length	4 s
Number of shots, bedrock/till	12/131

Table 3. Seismic data used for tomography.

Profile	Number of traveltimes	% of all data	Model size: x (m)	Model size: y (m)	Profile length (m)
1	22,650	87.1	3000	200	2950
2	18,042	83.1	2500	500	2740
3	13,185	92.2	250	2100	2050
4	14,437	73.6	300	2500	2410
5	47,167	93.0	1500	4700	5280

rections are, in theory, independent of how the velocity field is parameterized. The systems of equations for solving for the static corrections for the field data geometry are overdetermined and well behaved. After conversion to cover thickness, the error of the cover thickness estimates based on the computed data residuals are on the order of centimeters. Clearly, this is an optimistic error estimate, which is also illustrated in Figure 3b, showing deviations from the true model up to several meters. The reason for this is that the linear standard error estimates do not take the nonlinear aspects of the problem into account. The other main sources of errors are that we assume it is correct to initially assume the statics are associated with just the receivers (or sources) and that all rays travel vertically through the overburden layer. We have designed our approach to avoid the slow velocity cover being smeared into the bedrock velocities for them to be as exact as possible. However, some smearing will still occur, which will degrade the accuracy of the cover thickness estimates. In a real case, the velocities in the cover will only be approximately known. Instead of trying to quantify each of those sources of errors, we use the results of the synthetic example to provide reasonable error estimates of the cover thickness estimates. We believe this is a reasonable approach, as we have designed the example to be similar to our real case, e.g., in terms of expected traveltime errors, and that the inversion could never recreate the true model because of the coarser model discretization and the applied smoothing constraints. The mean difference between the reconstructed and true low-velocity cover thickness is 1.05 ± 0.64 m (one sigma). This indicates that our approach may underestimate the cover thickness, on the order of 1.69 m (one sigma). This is also supported in the comparison with the few borehole measurements (Table 5).

RESULTS

Where the depth to bedrock is shallow, the tomographic results can be compared directly to the information from the shot holes (Figures 5 and 6). However, because the maximum depth of these shot holes is limited to 1.5 m, other data are needed to confirm the tomography where the cover is thicker. Because of the comprehensive investigation program associated with the site studies, numerous core and hammer boreholes have been drilled in the area (Figure 4) to assess the bedrock from the near surface down to about 1000 m depth. Some of these boreholes were positioned at, or close to, the location of the reflection seismic profiles. To estimate the depth to bedrock from the static corrections, a velocity function is required.

We assigned a 1D velocity function (Table 4) for three reasons. First, the Quaternary deposits are generally similar throughout the area. Second, the three short refraction surveys revealed a structure consisting of three layers with rather similar velocities from site to site. Third, the thickness of the layers varied between the three sites so that any attempt to make a 2D model would have required complete refraction surveys along all five profiles. Measured depths to bedrock (Figures 5 and 6, and Table 5) for boreholes in the area close to the seismic profiles agree well with estimates using our tomographic scheme, except for boreholes 1, 2, 7, 14, and 15. These boreholes with poor agreement are located more than 25 m away from the profiles and where there is no coverage in the model because of the acquisition geometry. Although boreholes farther away than 20 m from the profiles obviously cannot be used to confirm tomography estimates, they do indicate that cover thickness variations along the profiles and variations in the offset direction of the profiles are similar. The tomographic velocity models generally correlate with the reflectivity patterns in the stacked reflection seismic sections (Figures 5 and 6). Note that the stacked sections are not migrated, because many of the reflections originate from out of the plane of the profiles. The top 40–50 m of the stacked seismic sections lack information; a direct comparison between tomographic velocities and reflections is therefore impossible. Instead, we look at the reflectivity in the stacked section and project the reflections to the surface and compare these areas with the tomographic velocities at these locations. The stacked sections of Figure 5a and b show no distinct reflectivity near the surface. Variable velocities in the tomographic images of Figures 5c and 6a–c coincide with clear reflectivity in the stacked sections. In Figure 5c, three reflections may be projected up to the surface at 600, 1200, and 1850 m along the profile. These three reflections correspond to fracture zones as confirmed by borehole studies in the area (Juhlin and Stephens, 2006). The clearest reflec-

Table 4. The 1D velocity and layer thickness model for the loose unconsolidated sediments. Traveltime refers to one-way traveltime through the layer.

Layer	Thickness (m)	Seismic velocity (m/s)	Traveltime in layer (ms)
Top layer	0.9	450	2.0
Intermediate layer	2.5	1200	2.08
Bottom layer	Down to bedrock	3600	0.28

Table 5. Difference between estimated and measured depth for various borehole positions along the profiles.

Index	Measured depth (m)	Estimated depth (m)	Difference in depths (m)	Distance from profile (m)
1	12.2	2.6	9.6	29.9
2	12.0	2.5	9.5	30.7
3	3.2	3.1	0.1	22.5
4	2.3	3.1	−0.8	23.6
5	4.8	2.6	2.2	12.1
6	3.2	2.4	0.8	16.3
7	5.1	1.1	4.0	26.1
8	0.8	1.3	−0.5	5.2
9	6.6	5.6	0.9	19.8
10	2.5	2.8	−0.3	23.3
11	3.6	2.8	0.8	8.0
12	3.6	2.9	0.7	8.0
13	3.5	2.7	0.8	22.4
14	12.2	1.8	10.4	30.8
15	12.0	1.8	10.2	28.7
16	5.5	3.5	2.0	51.1
17	5.4	5.6	−0.2	64.2
18	3.4	1.4	2.0	39.5
19	2.0	1.6	0.4	49.7
20	2.5	1.4	1.1	35.8
21	2.1	1.1	1.0	21.8

tion, in Figure 5c, projects to the surface at 1200 m and corresponds to a low-velocity zone in the tomography Figure 6a does not have as clear reflections as Figure 5c; but at 1300–1600 m, where the velocity is lower, there are a number of weaker reflections projecting to the surface. Figure 6b and c has the strongest reflections on the stacked seismic sections and the most varying surface velocities. The strongest reflection projects to the surface at about 1350 m, corresponding to a significant decrease in the velocity in the tomographic section. The reflection that projects toward the surface at 1750 m in Figure 6b and c does not appear to correspond to a low-velocity zone in the tomographic model. However, the reflectivity also seems to terminate before reaching the surface. The low-velocity zones at 2250 and 2750 m correlate with reflections in the stacked seismic sections of Figure 6b and c. In summary, the velocity profiles show bedrock with a rather homogeneous velocity in the northwestern part of the study area. In the southeast, a more varied velocity field is present. These variations in velocity generally correlate with conspicuous reflections in the stacked seismic images.

DISCUSSION

Large velocity contrasts may pose an obstacle in some seismic applications but may be a requirement in others. In seismic tomography, the nonlinearity of the traveltime inversion implies that the larger the velocity contrasts, the more difficult it will be to obtain a good velocity model. The purpose of our seismic investigation is not to determine the internal structure of the cover but to determine the cover thickness of the glacial deposits and estimate the uppermost bedrock velocities. Tests on synthetic data show that this can be done using our TIS approach, that is, simultaneous tomographic inversion of the velocity field and static corrections. This works when all shots are located in the bedrock (set I) but also when the shots are located in the cover (set II) if a modified approach is used. When both the receivers and sources are in the cover, the inversion must be conducted in three steps to obtain a velocity model that agrees with the true model. In this case, static shifts from both the sources and receivers contribute to the traveltime delays. Therefore, we assigned half of the computed receiver statics to the shots and applied them to the traces in a surface consistent manner, improving the velocity field. The resulting static corrections that compensate for the delays of the rays passing through the low-velocity cover are then more appropriate than if all static shifts are associated only with the receivers. Comparison of the uppermost bedrock velocities shows that some of the wide zones

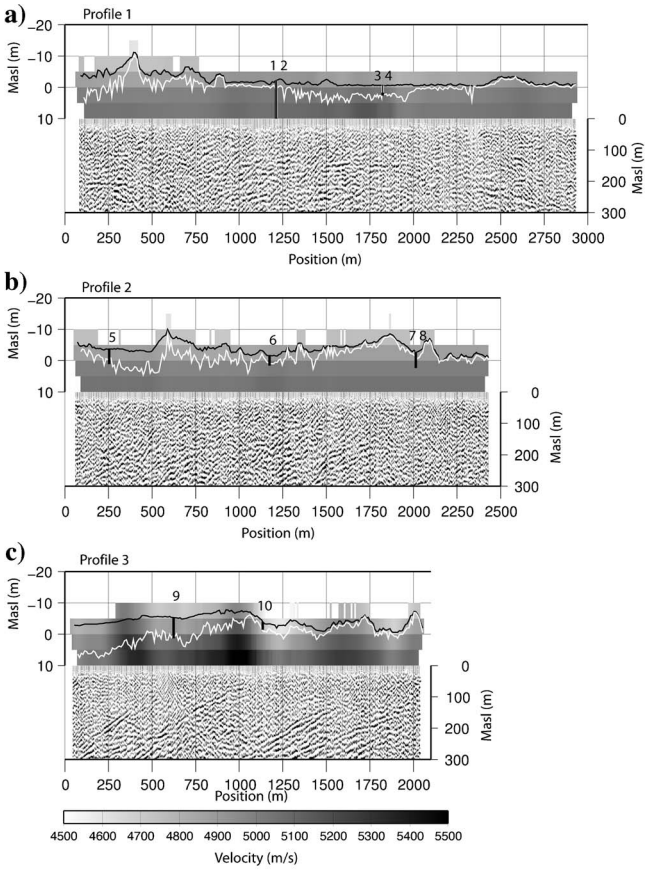

Figure 5. Velocities and estimated bedrock topography for a-c; surface topography (black line); estimated bedrock topography (white line). Boreholes (vertical black bar) are numbered as listed in Table 5. Stacked reflection seismic sections were depth converted with a constant velocity of 5000 m/s. M_{sal} = meters above sea level.

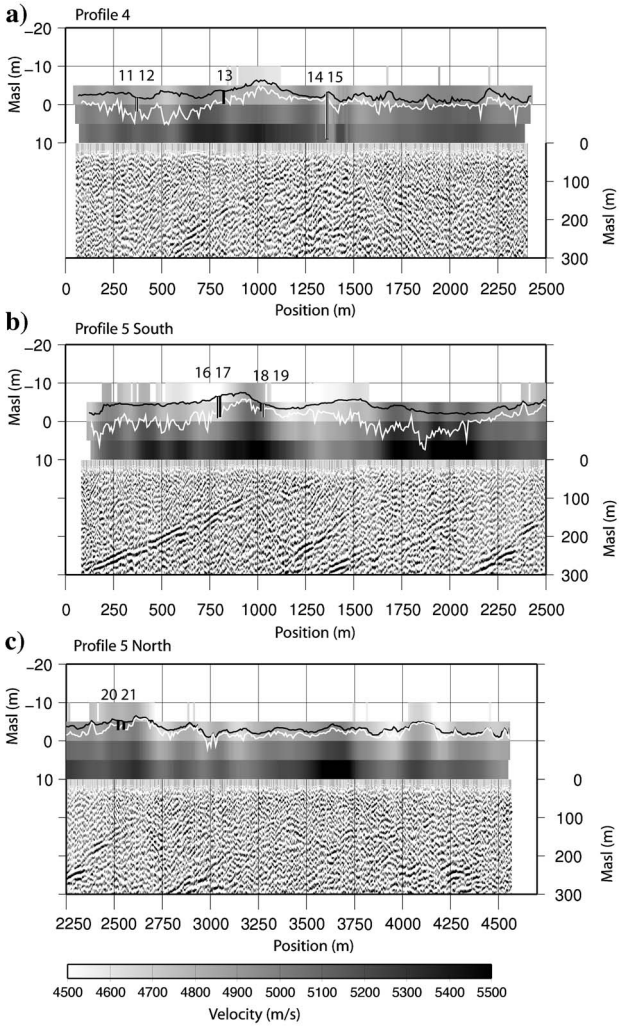

Figure 6. Velocities and estimated bedrock topography for (a) and (b); surface topography (black line); estimated bedrock topography (white line). Boreholes (vertical black bar) are numbered as listed in Table 5. Stacked reflection seismic sections were depth converted with a constant velocity of 5000 m/s. M_{sal} = meters above sea level.

of low velocities present in the tomographic image do not always correlate with reflections. This suggests that smoothing of the velocity field may still be a problem. In addition, the smoothing constraints required by the inversion will hinder the cover-bedrock interface from being properly modeled. Static shifts (tomostatics) computed from a model derived without simultaneous statics inversion underestimate the cover thickness and will lack the rapid bedrock variations typical in crystalline bedrock environments. Neither reducing the smoothing applied in the inversion nor increasing the depth to which the tomostatics were computed improved the results.

CONCLUSIONS

Our study shows that the first-break picks from reflection seismic data, acquired for site investigations for nuclear waste storage in crystalline rock can be used to obtain reliable information on the cover thickness and uppermost bedrock velocities. Synthetic data tests show that we can produce reliable velocity models even with a large velocity discontinuity at the cover-bedrock interface by using statics calculated simultaneously with the velocity inversion TIS. This is achieved even though we can only solve for receiver or source statics in one iteration at a time, not both at once. Velocity models such as those presented help close the information gap between the surface and the shallowest imaged reflections. Two synthetic test cases show that tomostatics do not produce as accurate a solution for the cover thickness and bedrock velocity as our proposed method. Tomostatics consistently underestimate the delay times, leading to estimates that are too small for the cover thickness. In a previous study, a data set in which all shot points were below the cover was analyzed. This study shows that the TIS method can be applied to field data where the shot points are in the cover itself. When applied to real data, TIS shows a good correlation of the estimated bedrock depth with depths found in boreholes located close (less than 25 m) to the profiles. We suggest the correlation length of the bedrock topography is a few tens of meters. Finally, bedrock velocities are more homogeneous in the northwestern part of the study area. In the southeast, low-velocity bedrock generally correlates with seismic reflections that project to the surface, supporting the interpretation that these reflections originate from fracture zones.

ACKNOWLEDGMENTS

We thank SKB for funding parts of this study. Niklas Linde is gratefully acknowledged for his input in this paper. Associate editor Aldo Vesnaver and four anonymous reviewers are greatly thanked for their suggestions and creative criticism of the manuscript, which improved the presentation of this study.

REFERENCES

Benz, H. M., B. A. Chouet, P. B. Dawson, J. C. Lahr, R. A. Paige, and J. A. Hole, 1996, Three-dimensional P and S wave velocity structure of Redoubt Volcano, Alaska: Journal of Geophysical Research, **101**, 8111–8128.

Bergman, B., H. Palm, and C. Juhlin, 2004a, Forsmark site investigation — Estimate of bedrock topography using seismic tomography along the reflection seismic profiles in Forsmark: Swedish Nuclear Fuel and Waste Management Company (SKB) Technical Report SKB P-04-99.

Bergman, B., A. Tryggvason, and C. Juhlin, 2004b, High-resolution seismic tomography incorporating static corrections applied to a till covered bedrock environment: Geophysics, **69**, 1082–1090.

Flecha, I., D. Marti, R. Carbonell, J. Escuder-Viruete, and A. Perez-Estaun, 2004, Imaging low-velocity anomalies with the aid of seismic tomography: Tectonophysics, **388**, 225–238.

Green, A. G., and J. A. Mair, 1983, Subhorizontal fractures in a granitic pluton — Their detection and implications for radioactive waste disposal: Geophysics, **48**, 1428–1449.

Hole, J. A., 1992, Nonlinear high-resolution three-dimensional seismic traveltime tomography: Journal of Geophysical Research, **97**, 6553–6562.

Hole, J. A., and B. C. Zelt, 1995, 3-D finite-difference reflection traveltimes: Geophysical Journal International, **121**, 427–434.

Juhlin, C., 1995, Imaging of fracture zones in the Finnsjön area, central Sweden, using the seismic reflection method: Geophysics, **60**, 66–75.

Juhlin, C., and H. Palm, 1999, 3D structure below Ävrö Island from high resolution reflection seismic studies, southeastern Sweden: Geophysics, **64**, 662–667.

Juhlin, C., H. Palm, and B. Bergman, 2002, Reflection seismic studies in the Forsmark area — Stage 1: Swedish Nuclear Fuel and Waste Management Company (SKB) Technical Report SKB TR-02-43.

Juhlin, C., and M. B. Stephens, 2006, Gently dipping fracture zones in paleoproterozoic metagranite, Sweden: Evidence from reflection seismic and cored borehole data, and implications for the disposal of nuclear waste: Journal of Geophysical Research, **111**, B09302.

Kim, J. S., W. M. Moon, G. Lodha, M. Serzu, and N. Soonawala, 1994, Imaging of reflection seismic energy for mapping shallow fracture zones in crystalline rocks: Geophysics, **59**, 753–765.

Kissling, E., 1988, Geotomography with local earthquake data: Review of Geophysics, **26**, 659–698.

Kissling, E., W. L. Ellsworth, D. Eberhart-Phillips, and U. Kradolfer, 1994, Initial reference models in local earthquake tomography: Journal of Geophysical Research, **99**, 19635–19646.

Lundin, L., E. Lode, J. Stendahl, P. M. Melkerud, L. Björkvald, and A. Thorstensson, 2004, Soils and site types in the Forsmark area: Swedish Nuclear Fuel and Waste Management Company (SKB) Technical Report SKB R-04-08.

Nielsen, L., H. Thybo, and L. Solodilov, 1999, Seismic tomographic inversion of Russian PNE data along profile Kraton: Geophysical Research Letters, **26**, 3413–3416.

Paige, C. C., and M. A. Saunders, 1982, An algorithm for sparse linear equations and sparse least squares: ACM Transactions on Mathematical Software, **8**, 43–71.

Pavlis, G. L., and J. R. Booker, 1980, The mixed discrete-continuous inverse problem: Application to the simultaneous determination of earthquake hypocenters and velocity structure: Journal of Geophysical Research, **85**, 4801–4810.

SKB, 2002, Forsmark — Site descriptive model version 0: Swedish Nuclear Fuel and Waste Management Company (SKB), Technical Report SKB R-02-32.

Squires, L. J., P. L. Stoffa, and G. Cambois, 1994, Borehole transmission tomography for velocity plus statics: Geophysics, **59**, 1028–1036.

Tryggvason, A., S. T. Rögnvaldsson, and Ó. G. Flóvenz, 2002, Three-dimensional imaging of the P- and S-wave velocity structure and earthquake locations beneath southwest Iceland: Geophysical Journal International, **151**, 848–866.

Vesnaver, A., F. Accaino, G. Bohm, G. Madrussani, J. Pajchel, G. Rossi, and G. Dal Moro, 2003, Time-lapse tomography: Geophysics, **68**, 815–823.

Wu, J. J., and R. F. Mereu, 1992, Crustal structure of the Kapuskasing uplift from Lithoprobe near-vertical and wide-angle seismic-reflection data: Journal of Geophysical Research, **97**, 17441–17453.

Yamamoto, T., 2001, Imaging the permeability structure within the near-surface sediments by acoustic crosswell tomography: Journal of Applied Geophysics, **47**, 1–11.

Zhu, X., D. P. Sixta, and B. G. Angstman, 1992, Tomostatics: Turning-ray tomography + static corrections: The Leading Edge, **11**, 15–23.